

## Liquid-solid contact electrification when water droplets hit living plant leaves

Serena Armiento <sup>1</sup>, Carlo Filippeschi<sup>1</sup>, Fabian Meder <sup>1,2</sup>✉ & Barbara Mazzolai<sup>1,2</sup>✉

Contact electrification has gained interest as a mechanism for generating charges on surfaces. It has also been shown that plant leaves generate electrification by both solid-solid and liquid-solid contact. However, it is unclear how water droplets hitting a leaf causes charging and which structural features affect this phenomenon. Here, we show how the in-situ surface structures of leaves, droplet composition, and prior ionization of the droplet influence living plant liquid-solid contact electrification on several superhydrophobic and hydrophilic living plant species. We find that the hierarchical structures responsible for self-cleaning and wetting, known as the Lotus effect, also create a specific electrification pattern. Each water droplet causes a characteristic signal in the plant tissue depending on the structure and composition of the epicuticular wax layer as well as the droplet composition. These findings give insight on how contact electrification occurs in nature, suggesting the potential for deriving new bio-based materials for sensing and energy harvesting in artificial and plant-hybrid devices.

<sup>1</sup>Bioinspired Soft Robotics, Italian Institute of Technology, 16163 Genova, Italy. <sup>2</sup>These authors jointly supervised this work: Fabian Meder, Barbara Mazzolai.  
✉email: [fabian.meder@iit.it](mailto:fabian.meder@iit.it); [barbara.mazzolai@iit.it](mailto:barbara.mazzolai@iit.it)

The outer surface of living plants especially leaves constitute the largest biointerface<sup>1</sup>. One of the most frequent events occurring on this interface is the impact of rain drops. Some plants (like from genus *Nelumbo*) established leaf surface structures that lead to superhydrophobic and self-cleaning behavior upon the water droplet–leaf collision, known as the famous Lotus effect<sup>2</sup>. Each droplet impact is connected with a mechanical energy that is transferred to the deformation of the liquid droplet and the elastic deformation of the leaf, petiole, and branch. Moreover, it was recently shown that mechanical solid–solid impacts on leaves are additionally translated into electricity by contact electrification occurring on the cuticle (the outermost polymeric layer expressed by the epidermis cells) causing surface charges which are induced into the inner conductive cellular tissue<sup>3–5</sup>. Depending on the materials which contact the leaf, this creates currents that can be harvested and used for powering low-power commercial electronics. Similar results have been achieved, using the living plant as part of the device and for example wind leaf fluttering as mechanical source energy or by extracting plant components or microstructures<sup>3–10</sup>. The mechanism is similar to what is exploited in artificial triboelectric generators based on engineered materials such as fluorinated ethylene propylene (FEP), polytetrafluoroethylene (PTFE), silicones, and e.g., polyamides like Nylon 6 as counter electrode, materials that create especially high contact charges<sup>11–14</sup>. A special case of contact or triboelectrification is liquid–solid contact electrification: the impact of liquid droplets on surfaces also leads to contact charging of the materials<sup>15–21</sup>.

Recently several experimental works have shed light on the mechanism of liquid–solid triboelectrification on artificial materials. It was suggested that the phenomenon involves both ion transfer and electron transfer, suggesting that the former is dominant on hydrophilic materials while the latter is dominant on hydrophobes<sup>22</sup>. The exchange of ions and/or electrons may occur as part of the electric double layer (EDL) formation<sup>22,23</sup>.

Similar to solid–solid triboelectrification, also liquid–solid triboelectrification was successfully turned into triboelectric nanogenerators (TENGs). The devices use the contact between flowing water as from raindrops, waves, or in water pipes and engineered materials to generate energy and to power small electronics, such as sensors and LEDs<sup>18,24–26</sup>.

Likewise, it was shown that water drops can produce electrical signals in plant-derived materials and on living leaves<sup>8,27</sup>. With an electrode assembled on the top of a leaf, such as shown by Zi et al.<sup>27</sup>, enhanced signals could be observed as the water droplet creates a varying capacitor during the impact. Yet, this requires additional electrodes onto which the droplet has to fall. Interestingly, the micro/nano structure of leaves have served as inspiration to make better performing artificial triboelectric nanogenerators, for example by imitating the surface hierarchical structure of water-repellent leaves, such as *Nelumbo nucifera*<sup>8,10,28–32</sup>. The lipids on the leaf surface have been shown to have a strong tendency to charge positively in solid–solid contacts, resulting in a placement in the triboelectric series even above artificial materials, like polyamides<sup>33</sup>. However, lignin components, interestingly, show a completely different behavior as highlighted by Baytekin et al.<sup>34</sup>; therefore, the diverse materials found in plants can result in different charging patterns and more information is needed on how contact charging occurs in nature. How liquid–contact electrification arises on the hierarchical, in-situ leaf surface of living plants remains unclear and how properties like superhydrophobicity, surface wax layers, and droplet properties at the water–leaf interface enhance it or reduce it.

Here, we investigated, liquid (water)–solid contact electrification on living plants as function of leaves' structural and wetting properties. Most experiments were performed using *Alocasia*

*macrorrhiza* and *Colocasia antiquorum*. Two species belonging to the same family Araceae and sharing some features but diverging in an important aspect: while *C. antiquorum* is water-repellent, *A. macrorrhiza* is hydrophilic. Comparing water droplet-induced leaf electrification revealed the fact that despite little affinity for the water droplet on the superhydrophobic species, the electrification by water contact is strongly increased. Selective removal of the epicuticular waxes and treatments which change their nanostructure strongly affected signal generation and elucidated the role of the wax layer in liquid solid contact electrification. The effect was confirmed by comparing other superhydrophobic and hydrophilic plants as well as artificial materials like fluorinated polymers. Experiments using artificially pre-charged water droplets and solutions with varying pH and ion concentration elucidated which factors affect liquid–solid contact electrification on living leaves. The results outlined in this paper give unprecedented insight into an event that occurs each time a rain drop falls on a leaf and has fundamental relevance for understanding liquid–solid contact electrification on complex surfaces in living organisms. Moreover, the results may serve as basis to develop a new generation of plant-hybrid devices such as plant-hybrid sensors and energy harvesting systems which aim for sustainable ecofriendly technologies for sensing plant status and plant health and thus ecosystem monitoring<sup>4,25,35–38</sup>.

## Results

**Selected plant species and their specific properties.** Figure 1a displays properties of the two model species. *A. macrorrhiza* and *C. antiquorum* have a similar overall leaf morphology, size, and shape. One of the most significant differences are the leaf surface properties and the correlated wetting behavior (Supplementary Table 1 summarizes possible biological functions of superhydrophobic leaves from literature). Figure 1b shows that the upper leaf surface of *C. antiquorum* has a water contact angle (CA) of  $\sim 150^\circ$  and is therefore superhydrophobic and water repellent, whereas *A. macrorrhiza* leaves are hydrophilic with a CA of  $\sim 80^\circ$ . Digital microscopy images of both species (Fig. 1c) reveal slight variations in the distribution and morphology of the epidermis cells in terms of size and shape. Scanning electron microscope (SEM) images show the presence of a dense layer of papillae (average size  $10.6 \mu\text{m} \pm 1.6$ ) and flat-platelet-shaped epicuticular waxes (average platelet thickness  $40 \text{ nm} \pm 10$ ) on the surface of *C. antiquorum* leaves, whereas the coverage of *A. macrorrhiza* is less dense consisting of single platelets (average platelet thickness  $120 \text{ nm} \pm 50$ ). The leaf section in which the wax layer was selectively stained in red (Fig. 1e) confirms the frequent presence of the waxes on *C. antiquorum*. These epicuticular waxes contribute significantly to the wetting behavior and the Lotus effect, described in detail elsewhere<sup>2,39–42</sup>.

The difference in the surface structure of *A. macrorrhiza* and *C. antiquorum* has expectedly an impact on the interaction of impinging water droplets on the leaves, as summarized by the high-speed camera snapshots in Fig. 2 and as further shown in Supplementary Movie 1. It is noteworthy that on both leaves, despite their different wetting properties, the droplets, after impact, spread to practically the same maximal expansion area (see Supplementary Fig. 1 for droplet expansion area and perimeter). The subsequent interaction differs for both species as highlighted in Fig. 2.

## Electric signals generated by water droplet–leaf interaction.

Figure 3a illustrates the schematic of the experimental setup for measuring liquid–solid contact electrification on whole living plants. A photograph of the setup can be found in Supplementary Fig. 2. The droplets were produced by a droplet generator that

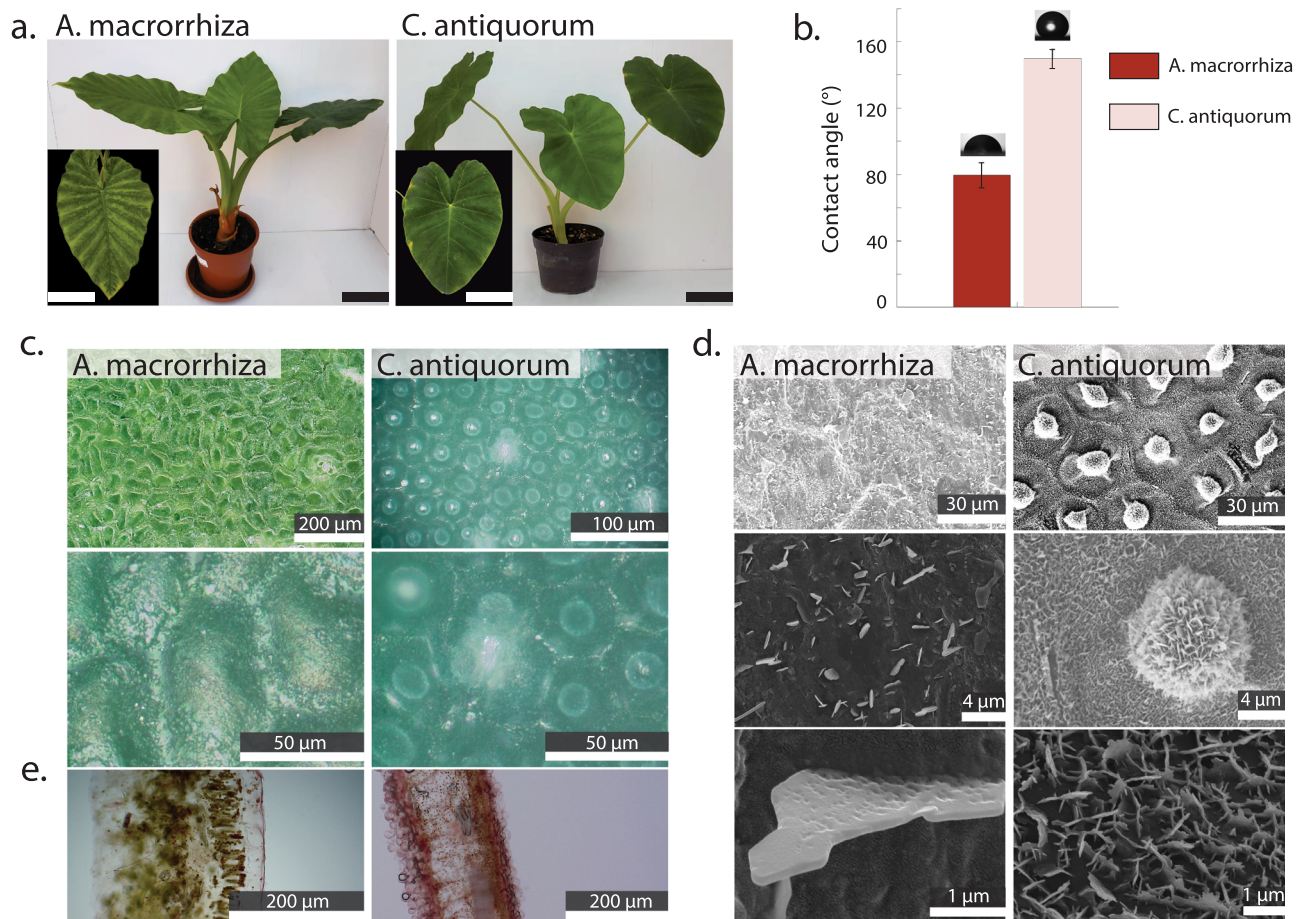


**Fig. 1** Characteristics of model species *A. macrorrhiza* and *C. antiqorum*. **a** Photographs of *A. macrorrhiza* and *C. antiqorum*, insets are top view images of the leaves. All scale bars are 10 cm. **b** Water contact angle of both species measured at 0° inclination. Mean and standard deviation of five measurements is given. **c** Digital microscopy of the adaxial side of the living leaf showing the surface and epidermal cellular structure. **d** SEM images of the adaxial leaf side at different magnifications showing the different distribution and density of surface wax crystals on both species. **e** Microscopy of leaf cross-sections of *A. macrorrhiza* and *C. antiqorum* and the cuticle specifically stained in red (using Sudan IV). The stronger red color of *C. antiqorum* samples qualitatively confirm the larger number of stained waxes.

allowed to control droplet volume and frequency (Supplementary Fig. 3) releasing droplets from a LDPE pipette with a metal outlet of the same diameter connected to electrical ground to avoid droplet charging prior to the impingement on the leaf. A Faraday cup was used to measure the charge of each individual droplet prior to its contact with the leaf to further check for any occurrence of unintended pre-charging of the droplet for example through friction with the pipette material<sup>23</sup>. The plant, the outlet of the droplet generator, and the Faraday cup were placed in a Faraday cage. The electrical signals were measured at an electrode inserted in the leaf petiole using the circuit illustrated in Fig. 3a. Figure 3b shows the current, charge, and voltage signals produced by 20 droplets sequentially impinging on a leaf of both species. High time-resolved signals of single droplets are shown in Supplementary Fig. 4. Moreover, we observed how the signals evolve with higher droplet numbers using up to 3500 droplets (Supplementary Fig. 5) showing that the signal for both plants are extremely stable (for some samples, especially artificial materials, as described later, a signal stabilization occurred at over 3000 droplets so that data was typically compared only after previously 3000 droplets contacted the surface).

The measurements clearly show a substantial difference in the current, charge, and voltage magnitudes generated. Typically, the current signals are at least 8.5 times higher for *C. antiqorum* than those of *A. macrorrhiza*. Figure 3c shows the absolute

amplitude of the signals. Also multiple tests using different plants of the same species and different leaves reproduced this behavior (Supplementary Fig. 6). Impedance spectroscopy of the ion-conductive cellular tissue (Supplementary Fig. 7a) reveals that the tissue impedance is of a comparable magnitude for both plants. This suggests that the conduction of the signals in the tissue is expected to be comparable and the observed difference in the electrical signals is not caused by the tissue acting as electrode and its impedance. Moreover, in all cases, the droplets were uncharged prior leaf impact as confirmed by the Faraday cup measurements (Supplementary Fig. 8) suggesting that the electrical signals are created during the mechanical impact on the cuticle and thus by liquid–solid contact electrification. As previously shown in Fig. 2, the droplet behavior on the *C. antiqorum* leaf is complex. In order to investigate how the different droplet-leaf surface motion states correspond to the signal formation, we tracked the droplet motion in high-speed and simultaneously with the current signal (Fig. 3d). Time duration from droplet impact to its maximum spreading, is only about 6 ms. The signal begins to develop shortly almost simultaneously with its maximum spreading and the current peak occurs after the maximum spreading, when the droplet already bursts and contracts/shrinks, reduces surface contact, and begins leaving the leaf. This suggests the mechanism depicted in Fig. 2e. When the droplet lands and spreads on the surface, contact electrification

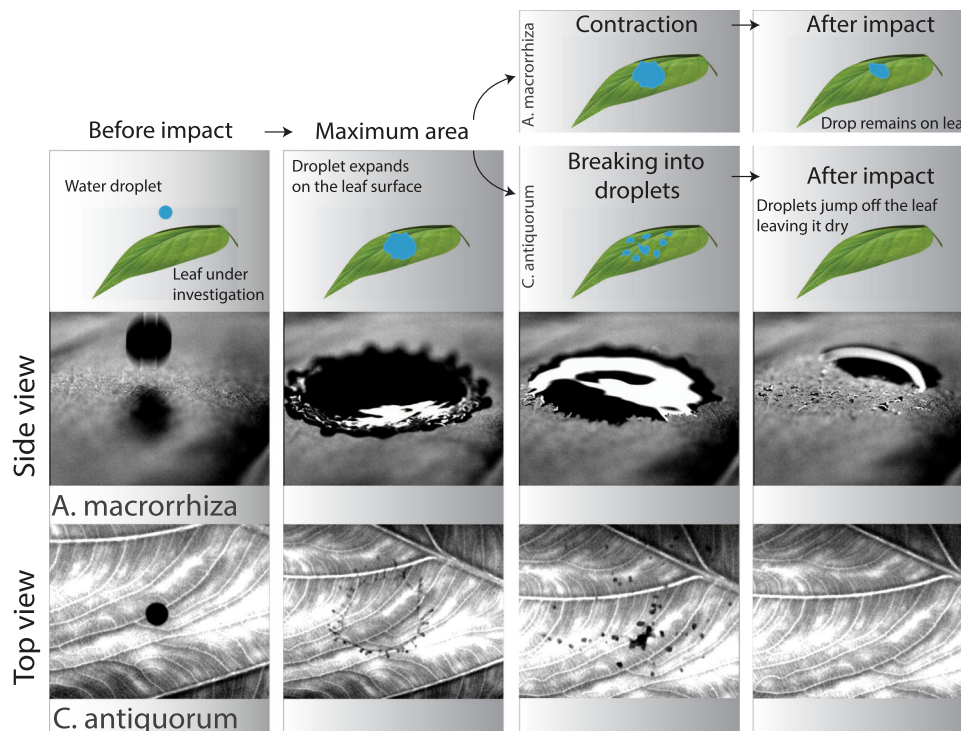


**Fig. 2 Wetting behavior of the two model species.** High-speed camera snapshots of the interaction between a water droplet and the surface of *A. macrorrhiza* and *C. antiquorum* leaves and illustrations of the different behavior of the two species. Videos of the droplet impact are given in Supplementary Movie 1.

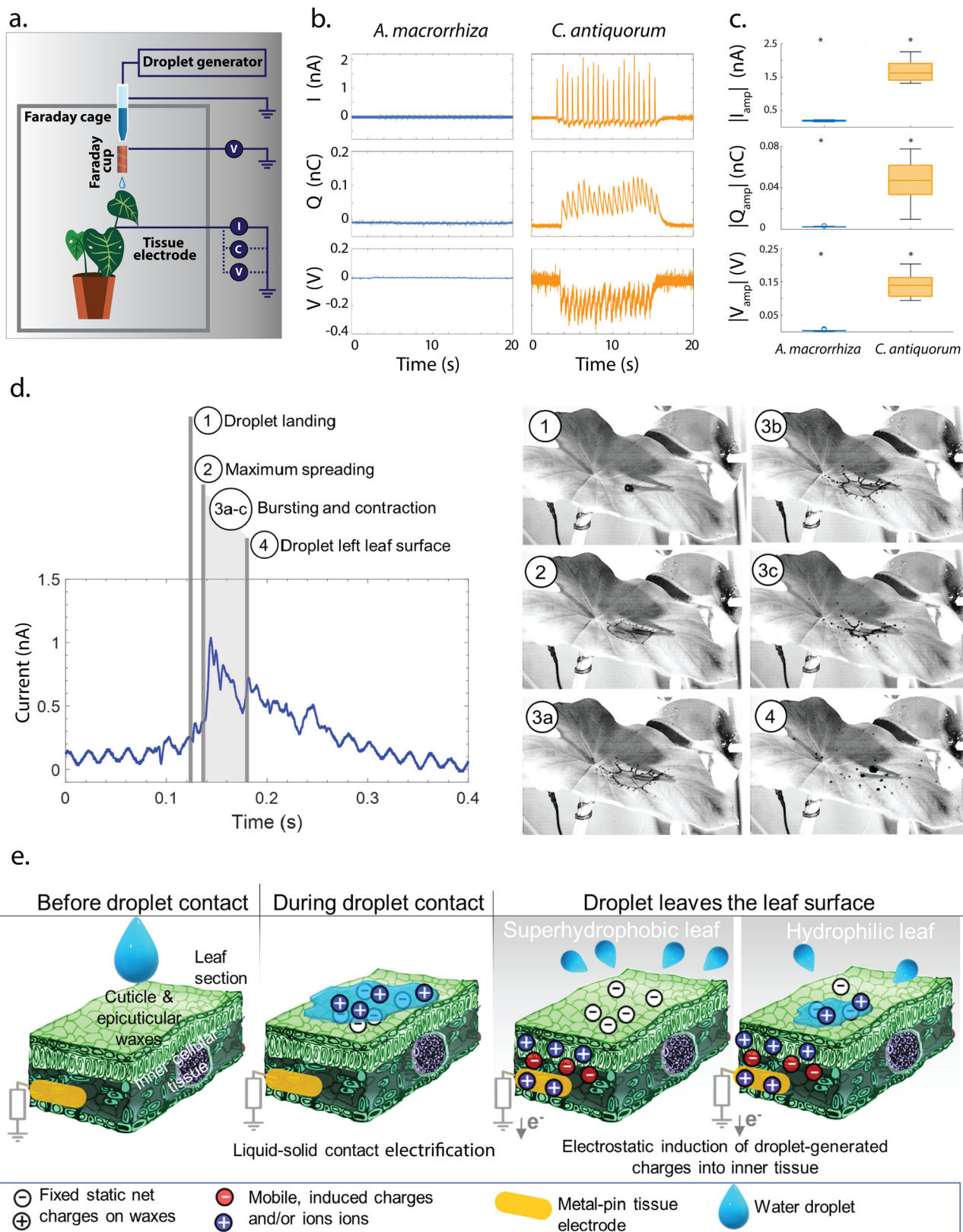
occurs and the droplet screens the generated charges. As soon as the droplet reduces surface contact, the charges become electrostatically induced into the inner tissue where the current is measured. On hydrophilic leaves the synchronization measurements were unsuccessful due to the too low signal amplitudes. Possible reason for these lower signals are (a) less charges form due to the different surface structure and (b) charges are screened by remaining water films as discussed later in detail.

**Electric signals generated by artificially pre-charged water droplets.** We then investigated how signals in both species evolve when the droplet itself carries a charge. Thus, the water droplet was artificially charged positively or negatively using an air ionizer at a distance of  $\sim 2$  cm applied from the water reservoir and removing the ground connection from the droplet outlet. When water droplets were expelled from the pipette, a positive or negative charge, respectively was left on the drop as indicated by the Faraday cup analysis (Fig. 4a). Figure 4b shows the mechanism and setup for pre-charging the droplets. It is assumed that when water comes into contact with the charged pipette surface, ions  $\text{H}_3\text{O}^+$ ,  $\text{OH}^-$  and other cations/anions, form an electrical double layer with excess positive or negative charges, respectively, depending on the net surface charge of the pipette<sup>23</sup>. As soon as a water droplet is dispensed from the charged pipette, excess positive/negative charges are dispensed with the droplet leaving behind the opposite negative/positive excess charge at the source, respectively. The Faraday cup measurements clearly display the passage of a charged object providing information on the droplet charge and the velocity of the droplet which, under these conditions, is about  $2.75 \text{ m s}^{-1}$ . Fig. 4a shows the current signals caused by charged droplets impacting on the plants reaching up to  $\sim 25 \text{ nA}$  and  $\sim 500 \text{ mV}$  (corresponding voltage and charge measurements are given in Supplementary Fig. 8). Several effects can be observed: if the droplet is positively charged, the current signal has an initial larger negative peak, and vice versa, if the

droplet is negatively charged, it causes an initially positive current peak. Moreover, the signals reduce in amplitude with the droplet number. This correlates with the reduction of surface charge on the droplets over time as also detected in the Faraday cup. The scatter plots in Fig. 4c clearly show that there is a linear positive correlation between the droplet charge amplitude and the current, voltage, and charge signals amplitude ( $C_{\text{Droplet}} \propto I_{\text{Leaf}}, V_{\text{Leaf}}, C_{\text{Leaf}}$ ) generated in the plant. Interestingly, the signals measured in the leaves are now almost the same for both species with similar amplitudes, or even higher amplitudes for *A. macrorrhiza* (reaching up to  $25 \text{ nA}$  and  $500 \text{ mV}$ ). Instead, when uncharged water droplets were employed, *A. macrorrhiza* generated only  $0.1 \text{ nA}$  and *C. antiquorum* up to  $2 \text{ nA}$  current peaks. Supplementary Fig. 9 gives the results when instead of DI water pre-charged  $1 \text{ M NaCl}$  is used, showing that introducing a high ionic strength does not dominate the signals due to pre-charging the droplets (different from signals caused by contact electrification which are strongly affected by ion strength as detailed later), The droplet pre-charge has thus a significant influence on the electrical signals generated. This confirms two hypotheses: (i) charges which transiently occur on the leaf surface (either due to liquid–solid contact electrification or droplet pre-charging) are induced into the ion-conductive inner leaf tissue acting as an electrode; (ii) if the droplet is uncharged, liquid–solid contact electrification, manifested as function of the leaf surface properties, plays the major role in the signal formation.

#### Influence of ion concentration and pH on the electric signals.

Next, we investigated the effect of the concentrations of monovalent ions ( $\text{NaCl}$ , Fig. 5a), and the pH (Fig. 5b) on the current signals caused by *C. antiquorum* (Fig. 5). Increasing the ion concentration causes a behavior with apparently clear partitions: for low concentrations ( $[\text{NaCl}] < 1 \text{ mM}$ ), increasing the ion concentration seems to enhance the signals compared to DI water, whereas for higher concentrations ( $[\text{NaCl}] > 1 \text{ mM}$ ), the



signal amplitudes are progressively suppressed. For a concentration of 1 M NaCl, the signals even switch the polarity. The lower signals of *A. macrorrhiza* (Supplementary Fig. 10) were less affected and did not show a polarity switching. Figure 5b shows the electrical signals of *C. antiquorum* leaves caused by deionized water or 1 M NaCl, respectively adjusted to pH 3, 6, and 11,

respectively. A clear effect of pH on the current signals can be noticed (ion concentration due to pH adjustment is about 1 mM) which may be related also to a damage of the wax layer as discussed later. No significant difference can be seen when 1 M NaCl at different pH is used suggesting that the ion concentration dominates the effect of the pH under these conditions.

**Fig. 3 Measuring water-droplet contact electrification in a living plant.** **a** Schematic of the experimental setup. **b** Current, charge, and voltage signals generated by twenty sequential droplet impacts on *A. macrorrhiza* (blue) and *C. antiqorum* (orange). **c** Absolute amplitudes of current, charge, and voltage signals of *A. macrorrhiza* (blue) and *C. antiqorum* (yellow) of 60 measurements (significantly different,  $\alpha = 0.05$ , Student's *T* test). All experiments have been performed with deionized water. **d** Time-domain synchronized analysis of droplet interaction and current signal formation in *C. antiqorum*. The images on the right are frames of high-speed camera recordings corresponding to the times of the signal formation. Supplementary Movie 2 shows a high-speed video of a synchronized recording. **e** Suggested mechanism for current signal formation based on liquid solid contact electrification and electrostatic induction of signals in the inner cellular tissue. The illustration of the leaf structure, charges, and electrode, was reproduced from ref. 3 with permission from Wiley 2018.

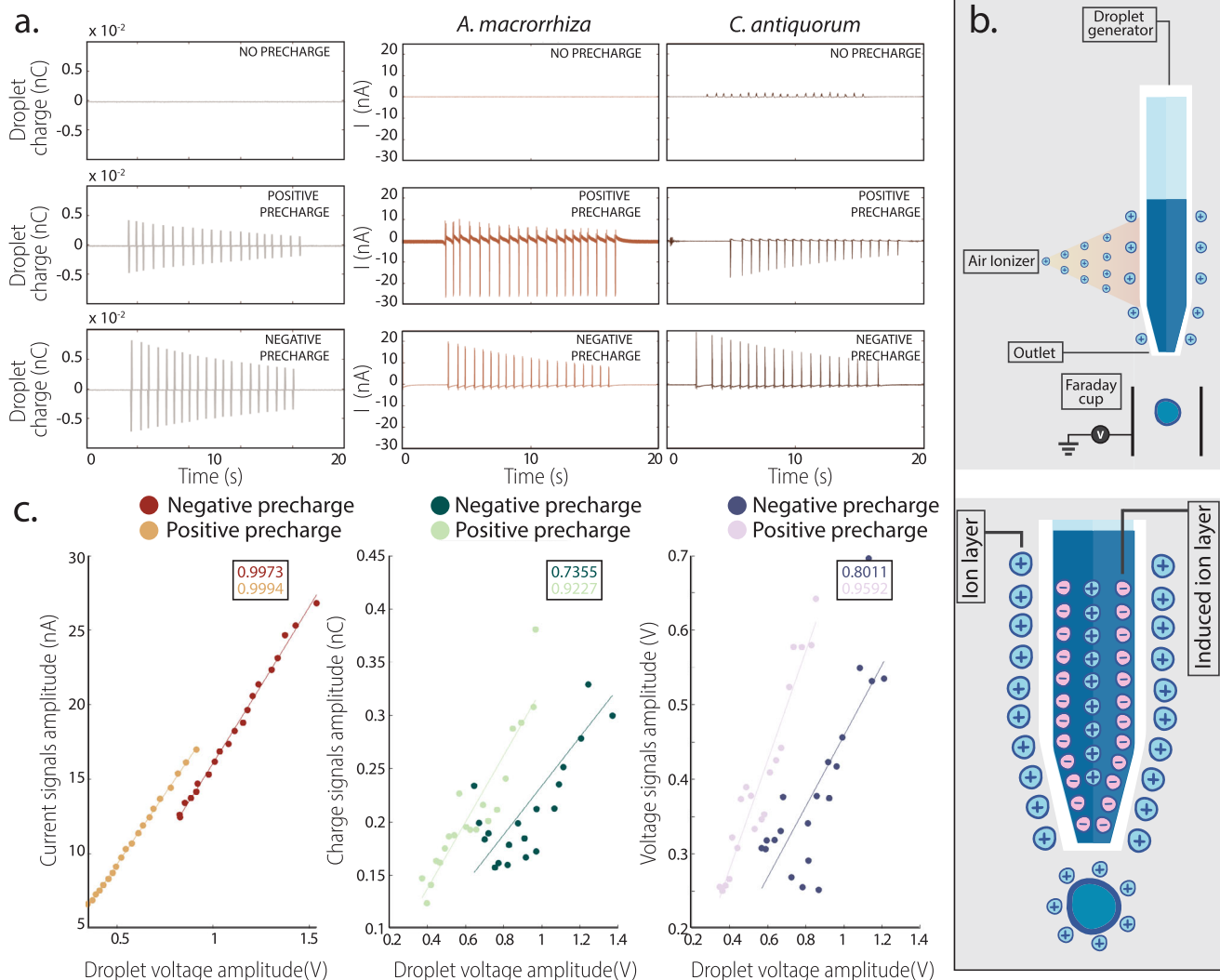


**Fig. 4 Effect of droplet pre-charging on the signals generated in *A. macrorrhiza* and *C. antiqorum*.** **a** Table of graphs showing the droplet charge before leaf impact (first column), current signals measured in *A. macrorrhiza* (second column) and *C. antiqorum* (third column). The first row corresponds to no pre-charge condition, the second to positive pre-charge and the third to negative pre-charge. Each electrical variable was measured thrice per leaf, for a total of 60 droplets and signals; results of 20 droplets are representatively shown. **b** Schematics showing the setup (upper panel) and the mechanism (lower panel) of droplet pre-charging by pipette ionization. **c** Scatter plots illustrating the relationship between the droplet signal in the Faraday cup and the current, charge, and voltage amplitudes in *C. antiqorum*. Each point corresponds to a single droplet impact in a series of twenty sequential impacts. The insets give the correlation coefficients between the droplet voltage signal measured in the Faraday cup and the corresponding current, charge or voltage; a linear fit for each set is included.

**Influence of selective melting and removal of epicuticular waxes.** A specific experiment was then designed to investigate the influence of epicuticular waxes on the electrical signals generated by *C. antiqorum*. Therefore, the electrical signals of an untreated leaf were compared with that of the same leaf after (1) gentle melting of the waxes nanostructure resulting in a flatter

epicuticular wax layer and (2) removal of the epicuticular waxes through a chloroform treatment. SEM images in Fig. 6a clearly confirm the successful melting and removal of the epicuticular waxes and show that the epidermis and papillae remained after treatment. Digital microscopy images using reflected light further suggest the melted wax layer by showing a shinier leaf surface

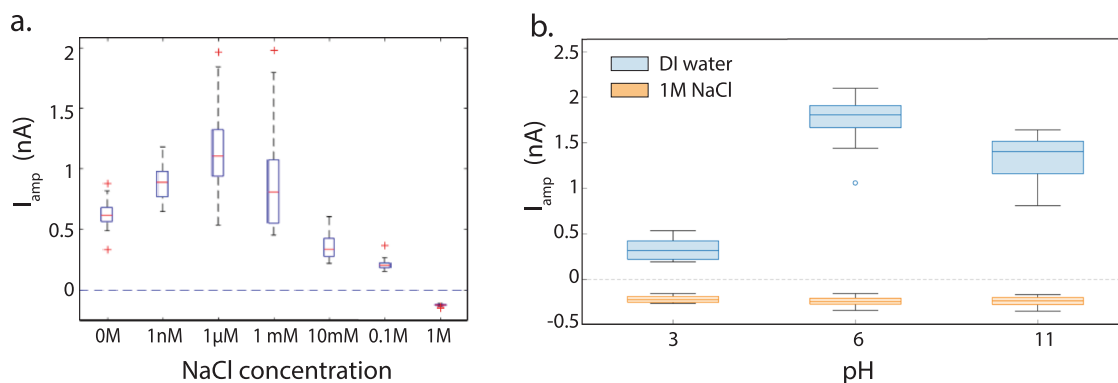


**Fig. 5** Effect of liquid's monovalent ion concentration and pH on electric signals generated after contact with *C. antiquorum*. **a** Boxplot showing the effect of NaCl concentration on the generated current amplitude. Each box represents 50 measurements recorded after previously 3000 droplets of the same solution have been dropped on the leaf. **b** Effect of pH on the generated current amplitude. The boxplot summarize 20 droplet impacts on *C. antiquorum* leaves for each ion concentration and pH, respectively.

(Supplementary Fig. 11). FTIR measurements (Supplementary Fig. 12) before and after wax removal confirmed a reduction of the vibrations at  $1460\text{ cm}^{-1}$ ,  $1470\text{ cm}^{-1}$ , and  $719\text{ cm}^{-1}$  which correspond to structures present in the cutin and the waxes<sup>43</sup>. Moreover, both, the epicuticular wax melting or removal caused a reduction of the contact angle by  $\sim 30^\circ$  (Fig. 6c) compared to the pristine leaf. Yet, the contact angle remains high at  $\sim 120^\circ$  and the droplet interaction with the treated leaf surfaces was still hydrophobic and not comparable with that of the hydrophilic *A. macrorrhiza* leaf (Supplementary Movie 3). Both treatments have a clear effect on the electrical signals generated by the leaf's liquid–solid contact electrification (Fig. 6b). Removing the epicuticular wax layer strongly reduces the generated voltage signals caused by deionized water droplets from a current amplitude of about 1 nA to peaks of  $-0.1\text{ nA}$ . Just melting the waxes and changing the nanostructure to a flatter epicuticular wax layer also reduces the signals about twice in magnitude to an average amplitude of  $\sim 0.5\text{ nA}$ . More detailed voltage, charge, and current data of single droplets of the experiment summarized in Fig. 6b can be found in Supplementary Fig. 13. The results clearly suggests that the wax layer plays a major role in the signal formation whereas removing the waxes affects the signals stronger than its structural changes. It is also clear that although the treated leaves remained hydrophobic with contact angles of  $\sim 120^\circ$ , the signals reduced and hydrophobicity alone may not play the main role in signal formation. To assure that the variation in the signals is indeed due to the variation in the surface waxes, we confirmed that the treatments have only a marginal influence on the cellular tissue acting as electrode and impedance spectroscopy already given in Supplementary Fig. 7c reveals that the tissue impedance varies in the same order of magnitude and is not significantly affected by both treatments excluding a major impact on the signal magnitude. Therefore, the drastic reduction of amplitude of the signals as measured in the wax-modified *C. antiquorum*, is most likely the result of chemistry and structure of the surface waxes.

**Comparison with other plant species and artificial surfaces.** Subsequently, we compared the behavior of further plant species: three superhydrophobic species (*C. antiquorum*, *Nelumbo nucifera*, and *Tropaeolum majus*) and three non-hydrophobic species (*A. macrorrhiza*, *Hedera helix*, and *Nerium oleander*). Images of surface structures and contact angles of all species can be found in Supplementary Fig. 14 and recording of the leaf–droplet interactions in Movie 4). The results in Fig. 7 confirm that superhydrophobic species in general produced higher current amplitudes than hydrophilic species during droplet interaction

while less significant variations among the superhydrophobic or hydrophilic species, respectively occurred. Yet, due to the previous analysis on leaves with varied wax structure, the clear trend that superhydrophobic plants have higher signals than hydrophilic plants may not solely be caused by the hydrophobic/hydrophilic properties but by parameters of the wax layer such as micro/nanostructure, wax density, chemistry etc.

Moreover, we compared the electrical signals generated by artificial materials upon droplet interaction tested under the same conditions. Supplementary Fig. 15a shows an analysis of polyethylene terephthalate (PET), silicone rubber, fluorinated ethylene propylene (FEP), and polytetrafluoroethylene (PTFE) applied on a flexible indium-tin oxide (ITO) electrode. As expected, different amplitudes are achieved for the different material surfaces due to the expected material-dependency of liquid–solid contact electrification. Interestingly, although all artificial materials generated higher amplitudes than *C. antiquorum*, the current, voltage, and charge signals generated by this plant were still found within the same magnitude of those of, e.g., highly fluorinated artificial materials like PTFE.

## Discussion

Our results clearly confirm that living plant leaves are a platform that generates electrical signals upon contact with water droplets, either through contact electrification on the outer leaf or through pre-charged droplets landing on the leaf. In both cases, the charges received by the external leaf surface are electrostatically induced in the ion-conductive tissue.

When droplets are uncharged, cuticle contact electrification is significant cause of the electrical signal measured. Our results clearly show which factors of the leaf lead to higher or lower contact electrification upon droplet interaction. The effects are often deeply interconnected and mechanisms overlay on highly complex surfaces of the leaves. Yet, our results point to the following behavior.

First, clearly, the epicuticular wax layer plays an essential role. The two features especially affecting leaf's liquid contact electrification are (a) its nanostructure and (b) its specific chemistry. The latter was anticipated for solid–solid contact electrification of leaves found by Kim et al.<sup>33</sup>. Our results suggest that the wax presence and chemistry may play a more important role compared to its micro-/nanostructure as melting the waxes to achieve a flatter surface reduced the signals only about twice in *C. antiquorum*. However, removing the epicuticular waxes from the leaf reduced the signals tenfold. Moreover, the signals after wax-removal are reaching similar current, voltage and charge

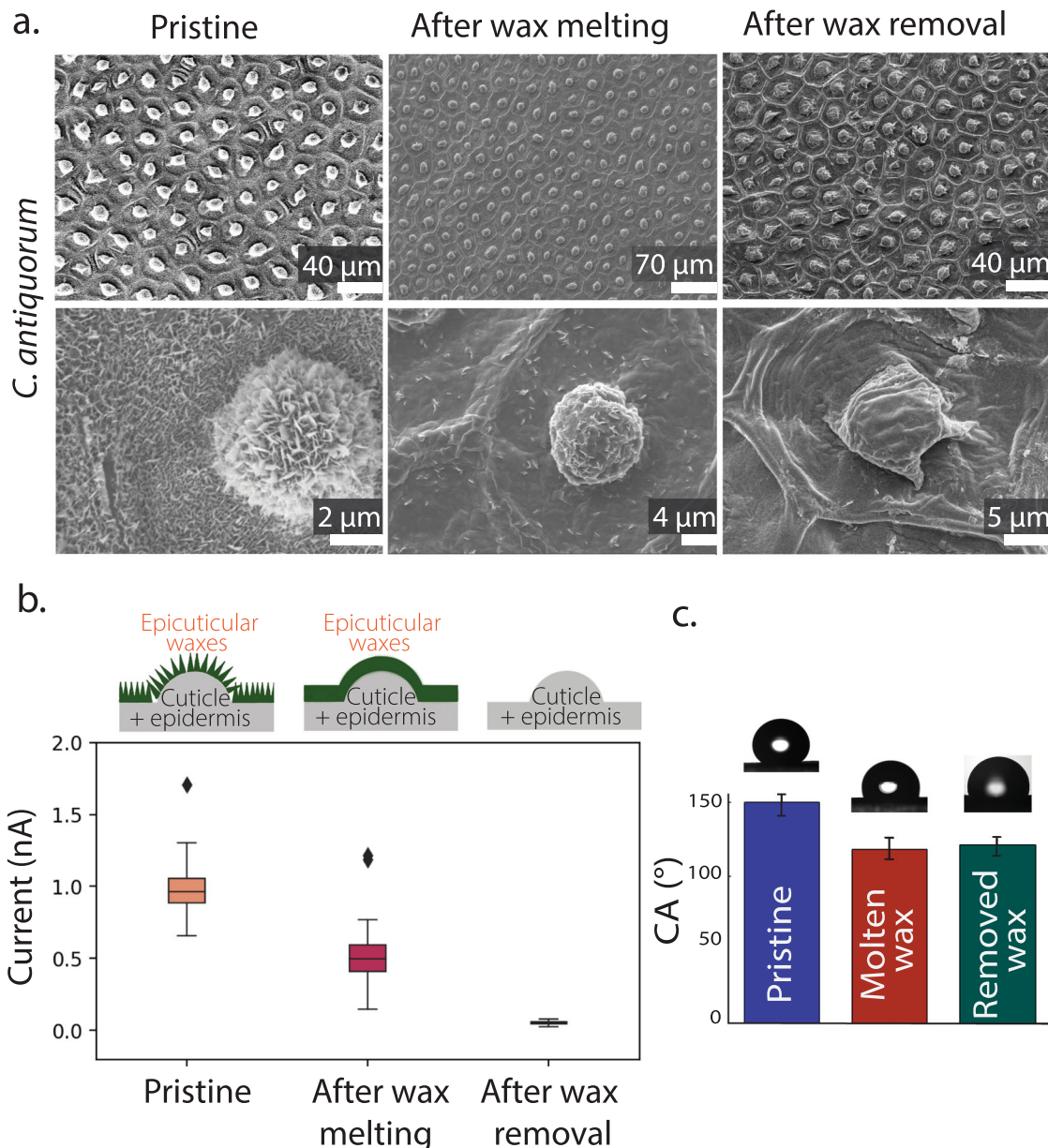


**Fig. 6 Influence of nanostructure and selective removal of epicuticular waxes on the water-droplet contact electrification of *C. antiquorum*.** **a** Scanning electron microscope (SEM) of a *C. antiquorum* leaf when pristine, when epicuticular waxes are gently melted and when the waxes are removed. **b** Comparison of electric signals on a *C. antiquorum* leaf with intact waxes, molten wax, and removed waxes, respectively. The statistics refer to 50 droplets for the pristine and molten leaf, while for the wax removal case they refer to 20 droplets. Single-droplet signals for current, charge, and voltage are given in Supplementary Fig. 12. The schematics on top of the graph illustrate the different morphology of the waxes in the three cases reported: intact wax crystals in the pristine leaf, molten waxes forming a flatter, continuous layer, and complete absence of epicuticular waxes. **c** Effect of the wax melting and wax removal on the water contact angle ( $N = 5$ ) of a *C. antiquorum* leaf. Standard deviation of five measurements is given.

magnitudes to those obtained from plants that do not have a similarly dense wax layer. This suggests that the removal has clearly a more significant effect than just morphological changes in the wax layer.

Second, another important aspect is the superhydrophobicity. Testing three superhydrophobic species showed that the signals obtained from those are generally higher than those obtained from the three hydrophilic species tested. However, superhydrophobicity/hydrophobicity alone is not a guarantee for high leaf-droplet contact electrification: experiments with removed wax layers in *C. antiquorum* still showed hydrophobic behavior (contact angles  $120^{\circ}$ ) but signals were low and similar to hydrophilic plants. This shows that, again, the presence of a

dense, nanostructured wax layer is more important than hydrophobicity even if these two properties are often connected in natural conditions. However, there is another crucial feature of superhydrophobic surfaces, this is their ability for self-cleaning and complete removal of water from the surface. On hydrophilic plants, instead, water layers remain and may partially screen charges affecting signal formation and induction<sup>8,9,16,27,44,45</sup>. Indeed, the contact time of the water droplet, the bouncing-off rates, and the remaining water films also play a role in liquid solid contact electrification<sup>46–48</sup>. Moreover, although the droplet spreading area on the hydrophilic *A. macrorrhiza* and the superhydrophobic *C. antiquorum* was similar, it is expected that the water-surface contact area is higher on the hydrophilic leaf



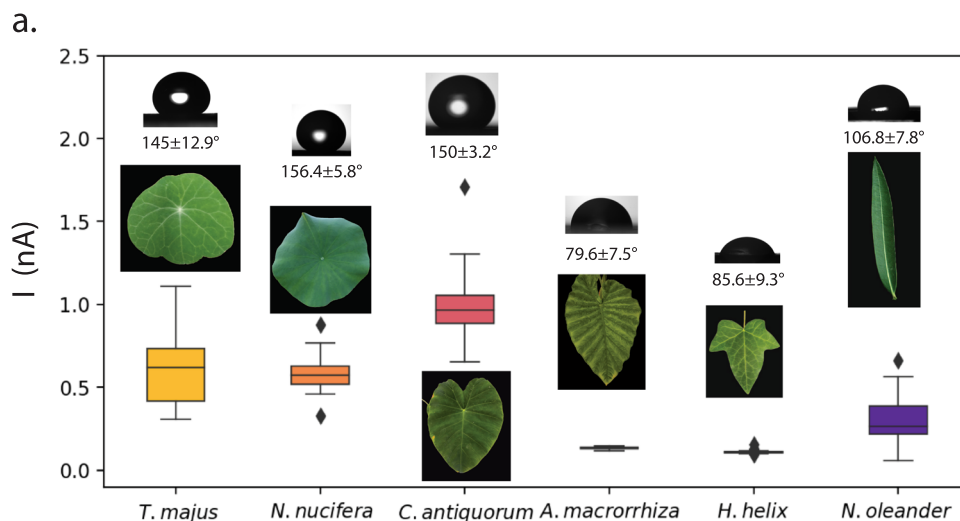


**Fig. 7 Comparison of water droplet contact electrification on different plant species.** Boxplot summarizing currents measured in fresh leaves of *N. nucifera*, *T. majus*, *C. antiqorum*, *H. helix*, *N. oleander* and *A. macrorrhiza* upon impact of DI water droplets. The statistics for all experiments have been obtained from 50 measurements of 50 droplets per datapoint (except for *T. majus* 20 droplets) recorded after initially 3000 droplets have sequentially been dropped onto the leaf to assure stable signals. Leaf photographs and contact angle for each species are reported as insets. Leaf-droplet interactions of the different species are given in Supplementary Movies 2 and 3.

surface especially on the microscale/nanoscale<sup>49,50</sup>. Increasing contact area is usually associated with higher leaf contact electrification and related signals<sup>3,51</sup>. There may be several reasons why this was not observed in our case, for example the remaining water layers screening charges as mentioned above or the fact that efficient contact with few points on the surface is already sufficient to create high contact charges (one fundamental charge in about 100'000 surface atoms (~1000 nm<sup>2</sup>) can yield thousands of volts as highlighted by Lacks et al.<sup>52</sup>). Here, again, the wax layers nanostructure with multiple sharp edges which are transiently contacted by the droplet could provide such points/hot spots.

Next, to the leaf properties, also the properties of the droplet played an essential role in the leaf liquid–solid contact electrification. The role of pre-charged droplets, as occurring for example in thunderstorms is discussed later. The signals generated by uncharged water droplets on *C. antiqorum* leaves were strongly affected by the ion strengths and the pH following thereby trends also reported for artificial materials<sup>22,53,54</sup>. Ion-rich solutions typically cause charge reduction by screening effects<sup>54,55</sup>. The previous increase with the ion concentration that we observed in the *C. antiqorum* leaves below 1 mM, seemed to be beneficial, e.g., an increasing droplet conductivity compared to deionized water as suggested in ref. <sup>54</sup>. Whereas then higher molarities caused a progressive decrease of the signals probably due to charge screening. Thus, superimposing effects may occur that do not always show a linear behavior and would need deeper investigation especially on complex leaf surfaces. Our results also show that the pH affects the signals amplitude. Whereas basic pH did not have a significant effect, at pH 3 (corresponding to an HCl concentration of 1 mM) signals significantly reduced. The pH expectedly has an influence on the liquid–solid contact electrification<sup>44,54</sup>. However, on leaves this is more complex. It was shown that exposure to pH 3 can significantly damage the epicuticular wax layer leading to a melted appearance as reported in ref. <sup>56</sup>. Thus, as we showed the strong effect of the wax layer on the signals when melting or removing the waxes, the signal reduction at low pH can be due to the damage of the wax layer. Yet, also in regards of occurrence of acidic rain in natural environments, a dedicated study of the complex effect of the pH in future would be interesting.

In addition, we observed that a solution of 1 M NaCl produced a polarity switch of the signals at all pHs. A possible explanation for

polarity switching could reside in the fact that electron and ion transfer could both contribute to the signal generation (yet it is not fully clarified which mechanism dominates in liquid–solid contact electrification even in less complex artificial materials)<sup>22,53</sup>. Increasing ion strengths were suggested to decrease the electron transfer whereas the ion transfer may not be significantly affected by the NaCl concentration<sup>22</sup>. Thus, this change in the contributions of both charge generation mechanism at high ionic strengths may manifest in a polarity change.

The comparison with artificial materials showed that plant leaves signals especially those of some superhydrophobic plants occur in a similar magnitude as signals obtained on artificial materials under the same conditions. The signals related to single rain drop impingements lead to voltage and current peaks of up to  $\sim 0.2 \pm 0.02$  V and  $\sim 2 \pm 0.2$  nA corresponding to  $\sim 0.4$  nW peak power while the current peak duration is about 60 ms at FWHM. These values suggest suitability for, e.g., sensing rain<sup>57</sup>. Moreover, if signals from multiple droplets add up, also energy harvesting may be considered, possibly by combining the output of multiple leaves and plants which will be part of a dedicated future study. Several further factors need to be taken into account, especially under outdoor conditions. The measurements were done under shielded, low noise conditions. Low signals, would be more difficult to distinguish without shielding or noise-filtering. However, under outdoor conditions a frequent phenomenon could be particularly beneficial and interesting to evaluate. Water droplets may charge<sup>58</sup> due to diffusion of atmospheric ions<sup>59</sup> and especially droplets in thunderstorms, are accompanied by formation of electric fields due to charge separation<sup>60</sup>. Moreover, the friction with the surrounding air produces charges on the surface of droplets<sup>61</sup>. We indeed showed that pre-charged droplets generate higher signals largely independent of the plant species and charges on the droplets are induced into the tissue where they can be harvested. The results thus clearly suggest the potential to derive new sustainable and eco-friendly, and plant-hybrid materials and solutions for such energy harvesters and sensors.

## Conclusions

Leaf-raindrop interactions are amongst the most frequent interactions that natural leaves experience. We have demonstrated using a bare, living plant without additional components except a

single electrode inserted in the stem that each droplet impact causes a characteristic electrical signal in the tissue especially on superhydrophobic plants. The results clearly demonstrate the fundamental role of the leaf epicuticular waxes on the signal generation, the droplet ion concentration, and pH. When droplets are uncharged and of low ion concentration, contact electrification causes the signals and signals are larger on densely wax-coated superhydrophobic plants. Yet, hydrophobicity alone does not enhance signals. Pre-charged droplets as they may occur in nature lead to even higher signals compared to those obtained from contact electrification. The results provide a base for further understanding the origin of liquid–solid contact electrification signals in living organisms like plants but also as inspiration for bioinspired artificial, or biohybrid energy harvesters and sensors.

## Methods

**Plant species and preparation.** *A. macrorrhiza* and *C. antiquorum* were purchased online from a plant nursery (Vivai Le Georgiche, Italy). The plants were kept in a growth chamber (MG322, Monti & Co., Italy) at average temperature of 27 °C, relative humidity (RH) of 47% and a photoperiod of 16 h. *N. nucifera* and *N. oleander* were purchased from a local plant nursery (Azienda Agricola Nymphæa Alba, Italy). Plants of *T. majus* were cultivated from seeds in soil for a period of about 5–6 weeks in the growth chamber. The leaves had reached full expansion at the time of the experiments. Plants of *H. helix* were derived from cuttings of existing plants in the area.

**Dedicated measurement set-up.** A Faraday cage was custom built using aluminum T-slot profiles and covered with copper mesh for electromagnetic shielding (Thorlabs Inc., NJ, USA). The cage was connected to electrical ground through an external cable. A Faraday cup of dimensions  $h = 11$  cm,  $d_{\text{int}} = 4$  cm and  $d_{\text{ext}} = 2.5$  cm was assembled using a sheet of brass and one of copper for the external and internal cylinders and silicone rubber for the separator. A droplet generator was designed and implemented in the setup as follows: a Peleus valve was connected to one end of a silicone rubber tube while the other end was connected to a PE pipette, equipped with an optional metal tip that allows electrical grounding of the outlet. The pipette and the tube were placed in the Faraday the cage in a way that the height could be modified according to the plant size.

**Electric measurements and droplet application.** A pin electrode connected through a cable to a high input impedance electrometer (6517B, Keithley, USA) was inserted in the petiole of the leaf chosen for stimulation. The Faraday cup was connected to an oscilloscope (MSO7014A, Agilent Technologies, USA) equipped with a passive 10 M $\Omega$  probe. Drops of deionized (DI) water (Elix<sup>+</sup> Advantage 10, Millipore SAS, FR) and sodium chloride (NaCl) solutions were employed for the experiments. When DI water and NaCl solutions were not pre-charged, the pipette outlet was grounded. The current (nA), charge (nC) and voltage (V) signals obtained from typically 20–60 droplets were recorded in a resolution of 20,000 datapoints per second. To assure that the signal of a sample stabilized at its maximum, we recorded how the signal develops over up to 5000 droplets, showing that after 3000 droplets the signals typically stabilized. Several samples (especially in *C. antiquorum* and *A. macrorrhiza*) showed stable signals over the whole range. Thus, to compare data between different samples, measurements were performed after 3000 droplets have impacted the surface. Signals of the Faraday cup and the leaf were recorded simultaneously. When performing saturation experiments or when stabilizing the output before some experiments, the Faraday cup was removed and a different droplet generator was employed: this was constituted by a drip-infuser connected on one side to a reservoir and on the other side to a metal outlet which was always grounded. A mechanical device allowed the regulation of the speed of droplets out of the outlet. In all experiments that used this setup the frequency set was of 1 drop per second, for a total of 50 droplets in a single set.

**Different droplet compositions.** NaCl (Analytical grade, ThermoFisher Scientific, Inc., USA) was mixed in indicated concentrations with DI water (Milli-Q<sup>®</sup> IQ 7003, Merck, Germany). The pH was adjusted with 0.1 M HCl (Fluka Analytical, USA) and 0.1 M NaOH (Sigma Aldrich, Germany) and measured with a pH meter (PC650, Eutech Instruments, ThermoFisher Scientific, Inc., USA).

**Tissue impedance spectroscopy.** Impedance spectroscopy was performed using an E4980A Precision LCR Meter (Keysight Technologies, USA). Two gold-coated pin electrodes were inserted in the plant tissue, one in the leaf tissue and one in the stem tissue. The position of the electrode in the stem to measure at different distances. The electrodes were penetrating the cuticle and contacting the inner ion-conductive cellular tissue. The complex impedance was measured at indicated frequencies (between 0.1 kHz to 1 MHz) applying a 1 V bias.

**Droplet pre-charging procedure.** In order to imprint an either positive or negative charge on the water droplets, an air ionization gun (Zerostat 3, Sigma Aldrich, Germany) was triggered and pointed towards the pipette containing the water causing the emission of a stream of positively (or negatively) ionized air. This was repeated three times before the experiment was conducted maintaining a constant distance between the gun and the pipette.

**Selective wax removal or melting.** To remove the epicuticular waxes of *C. antiquorum*, the upper leaf surface was washed multiple times with chloroform (99.8%, Sigma Aldrich, Germany) for a total period of ~30 s. A whole plant containing the treated leaf was then immediately used for experiments. To melt the waxes, a hot air gun (Multicomp Pro, Leeds, UK) was pointed perpendicular to the upper side of a *C. antiquorum* leaf for three seconds. The time was determined by preliminary experiments that showed that three seconds is the minimum time required to melt the waxes imparting as little damage as possible to the underlying leaf structure. For the experiments shown in this paper only a small portion of the lamina was treated and immediately tested or cut and observed under the scanning electron microscope.

**High-speed camera acquisition.** Droplet impacts on the subject leaves were recorded using a high-speed camera (Miro C110, Phantom High Speed, New Jersey, USA or MC1302, EOSense, Mikrotron GmbH, Germany) at over 1000 frames per second (fps) controlled by using a custom software programmed in LabVIEW (2018, National Instruments, USA). The videos were recorded with the camera in top and side view. Since the camera records monochrome frames, a drop of black water-based ink was used to increase the contrast.

**Synchronized tracking of droplet motion and voltage signal generation.** To track droplet motion states and signal formation, synchronization of high-speed videos and voltage registration was done as follows: when a droplet hits the leaf, part of its kinetic energy is transferred into the elastic deformation of the leaf blade. We positioned an electrode (1) under the leaf blade (fixed with dielectric double-sided tape to avoid electrical contact with the plant tissue) aligned with another electrode (2) fixed on a support in a distance of a few hundred micrometers from electrode (1). When the leaf is hit by a droplet, the two electrodes almost instantaneously touch due to the leaf deformation and close a circuit that generates a signal. This signal is recorded simultaneously with the triboelectric signals in the plant tissue using a multichannel oscilloscope. At the same time, we recorded the droplet interaction with a high-speed camera (Miro C110, Phantom High Speed, NJ, USA) at a framerate of ~1000 fps and observed (a) droplet spreading and (b) the moment when electrode 1 and 2 touch. The frame (when touch of electrodes 1 and 2 occurred) was used to synchronize video and electrical signals and could give real-time information on droplet deformation state and electrical signal.

**Fourier transform infrared spectroscopy.** Either fresh or dried leaves were analyzed with attenuated total reflection infrared spectrometer (MIRAcle 10, Shimadzu, Japan) in the 4000–600 cm<sup>-1</sup> range. The measurements were repeated ten times for each sample.

**Digital microscopy.** Fresh leaves of *A. macrorrhiza* and *C. antiquorum* were imaged through a KH-8700 digital microscope (Hirox, Japan). The same leaves were also cut in thin sections which were then stained for 10 min with 0.1% (w/v) solution of Sudan IV in isopropyl alcohol diluted 1:1 in water, then gently washed in 50% isopropyl alcohol. Afterwards the sections were mounted and immediately imaged.

**Scanning electronic microscopy.** Freshly picked leaves of *A. macrorrhiza* and *C. antiquorum* were cut in 1 cm<sup>2</sup> pieces and glued to SEM stubs with conductive carbon tape, which was also used to seal the edges, following a procedure described by Barthlott et al.<sup>62</sup> The so-prepared leaf samples were then sputter-coated with a thin layer of gold in a Gold/Carbon Sputter Coater (Q150RES, Quorum Tech, UK) and then imaged in two Scanning Electron Microscopes (EVO MA10, Zeiss, Germany and Helios NanoLab 600i, ThermoFisher Scientific, Inc., USA).

**Contact angle measurements.** Static contact angles were measured using an optical tensiometer (Attension Theta, Biolin Scientific AB, Sweden) after placing DI water droplets of diameter 500  $\mu$ m ( $V = 0.5$  mL) on freshly picked leaf samples that were taped with double-sided tape on microscope glass slides.

**Data and statistical analysis.** The measurement data was analyzed using MATLAB (2021 version, MathWorks, USA). Each experiment was repeated at least three times. One of the repeats containing typically 20–60 single droplets each was then selected for analysis for each acquisition (current, charge and voltage). A simple moving average over 50 points (on a total of a million datapoints) was applied to each file to remove background noise. This procedure did not influence signal peaks and amplitude analyzed here. The signal peaks were identified and

their amplitude was evaluated. Mean amplitude and standard deviation of the at least 20 peaks (corresponding to 20 droplets) were calculated.

For all the electric signal plots the average peak amplitude over 20 peaks was extracted together with its standard deviation. Box and whisker plots of all current signals were plotted to better visualize the differences between experimental conditions. Two-sample *t* tests (19 degrees of freedom) were carried out to evaluate the difference in the mean current between the two model species (under some experimental conditions) with a significance level of 5%. As described above, the charge of all droplets used for impingement during the experiments was measured using a Faraday cup. This was connected to an oscilloscope; therefore its raw data showed a voltage signal corresponding to the voltage difference caused at the two layers of the Faraday cup when a droplet (charged or uncharged) was passing through it. By using elementary concepts of charge induction in a cylinder (the external part of the cup is connected to ground), it was possible to estimate the corresponding droplet charge from the voltage signal read by the oscilloscope<sup>63</sup>.

## Data availability

The data supporting the findings of this study are available from the corresponding authors.

Received: 5 January 2022; Accepted: 5 October 2022;

Published online: 25 October 2022

## References

- Morris, C. E. & Kinkel, L. L. *Fifty Years of Phyllosphere Microbiology: Significant Contributions to Research in Related Fields* (American Phytopathological Society (APS Press), 2002).
- Barthlott, W. & Neinhuis, C. Purity of the sacred lotus, or escape from contamination in biological surfaces. *Planta* **202**, 1–8 (1997).
- Meder, F. et al. Energy conversion at the cuticle of living plants. *Adv. Funct. Mater.* **28**, 1806689 (2018).
- Meder, F. et al. Living plant-hybrid generators for multidirectional wind energy conversion. *Energy Technol.* **8**, 2000236 (2020).
- Jie, Y. et al. Natural leaf made triboelectric nanogenerator for harvesting environmental mechanical energy. *Adv. Energy Mater.* **8**, 1703133 (2018).
- Chen, Y. et al. Triboelectrification on natural rose petal for harvesting environmental mechanical energy. *Nano Energy* **50**, 441–447 (2018).
- Sun, J. G. et al. A leaf-molded transparent triboelectric nanogenerator for smart multifunctional applications. *Nano Energy* **32**, 180–186 (2017).
- Choi, D. et al. Spontaneous occurrence of liquid-solid contact electrification in nature: toward a robust triboelectric nanogenerator inspired by the natural lotus leaf. *Nano Energy* **36**, 250–259 (2017).
- Jeon, S. B., Kim, D., Yoon, G. W., Yoon, J. B. & Choi, Y. K. Self-cleaning hybrid energy harvester to generate power from raindrop and sunlight. *Nano Energy* **12**, 636–645 (2015).
- Seol, M. L. et al. Nature-replicated nano-in-micro structures for triboelectric energy harvesting. *Small* **10**, 3887–3894 (2014).
- Wang, S. et al. Molecular surface functionalization to enhance the power output of triboelectric nanogenerators. *J. Mater. Chem. A Mater.* **4**, 3728–3734 (2016).
- Bian, Y. et al. Triboelectric nanogenerator tree for harvesting wind energy and illuminating in subway tunnel. *Adv. Mater. Technol.* **3**, 1700317 (2018).
- Zhu, G. et al. A shape-adaptive thin-film-based approach for 50% high-efficiency energy generation through micro-grating sliding electrification. *Adv. Mater.* **26**, 3788–3796 (2014).
- Lin, Z. H. et al. A multi-layered interdigitative-electrodes-based triboelectric nanogenerator for harvesting hydropower. *Nano Energy* **15**, 256–265 (2015).
- Helseth, L. E. & Guo, X. D. Contact electrification and energy harvesting using periodically contacted and squeezed water droplets. *Langmuir* **31**, 3269–3276 (2015).
- Wang, Y., Gao, S., Xu, W. & Wang, Z. Nanogenerators with superwetting surfaces for harvesting water/liquid energy. *Adv. Funct. Mater.* **30**, 1908252 (2020).
- Lin, Z. H., Cheng, G., Lee, S., Pradel, K. C. & Wang, Z. L. Harvesting water drop energy by a sequential contact-electrification and electrostatic-induction process. *Adv. Mater.* **26**, 4690–4696 (2014).
- Xu, W. et al. A droplet-based electricity generator with high instantaneous power density. *Nature* **578**, 392–396 (2020).
- Wu, H., Mendel, N., van den Ende, D., Zhou, G. & Mugele, F. Energy harvesting from drops impacting onto charged surfaces. *Phys. Rev. Lett.* **125**, 078301 (2020).
- Zhu, H. R. et al. Self-powered metal surface anti-corrosion protection using energy harvested from rain drops and wind. *Nano Energy* **14**, 193–200 (2014).
- Zhang, Q. et al. A single-droplet electricity generator achieves an ultrahigh output over 100 V without pre-charging. *Adv. Mater.* **33**, 2105761 (2021).
- Lin, S., Xu, L., Chi Wang, A. & Wang, Z. L. Quantifying electron-transfer in liquid-solid contact electrification and the formation of electric double-layer. *Nat Commun* **11**, 399 (2020).
- Nauruzbayeva, J. et al. Electrification at water-hydrophobe interfaces. *Nat Commun* **11**, 5285 (2020).
- Wang, Z. L., Jiang, T. & Xu, L. Toward the blue energy dream by triboelectric nanogenerator networks. *Nano Energy* **39**, 9–23 (2017).
- Lan, L. et al. Breathable nanogenerators for an on-plant self-powered sustainable agriculture system. *ACS Nano* **15**, 5307–5315 (2021).
- Lu, Y. et al. A filter paper-based nanogenerator via water-drop flow. *Adv. Sustain. Syst.* **3**, 1900012 (2019).
- Wu, H. et al. Fully biodegradable water droplet energy harvester based on leaves of living plants. *ACS Appl. Mater. Interfaces* **12**, 56060–56067 (2020).
- Zhou, Q. et al. High humidity- and contamination-resistant triboelectric nanogenerator with superhydrophobic interface. *Nano Energy* **57**, 903–910 (2019).
- Jang, D. et al. Force-assembled triboelectric nanogenerator with high-humidity-resistant electricity generation using hierarchical surface morphology. *Nano Energy* **20**, 283–293 (2016).
- Yoo, D. et al. Biomimetic anti-reflective triboelectric nanogenerator for concurrent harvesting of solar and raindrop energies. *Nano Energy* **57**, 424–431 (2019).
- Cho, H. et al. Toward sustainable output generation of liquid-solid contact triboelectric nanogenerators: The role of hierarchical structures. *Nano Energy* **56**, 56–64 (2019).
- Chen, X. et al. Transparent and stretchable bimodal triboelectric nanogenerators with hierarchical micro-nanostructures for mechanical and water energy harvesting. *Nano Energy* **64**, 103904 (2019).
- Kim, D. W., Kim, S. W. & Jeong, U. Lipids: source of static electricity of regenerative natural substances and nondestructive energy harvesting. *Adv. Mater.* **30**, 1804949 (2018).
- Özel, M. et al. Why does wood not get contact charged? Lignin as an antistatic additive for common polymers. *Chem. Mater.* **32**, 7438–7444 (2020).
- Fiorello, I. et al. Plant-like hooked miniature machines for on-leaf sensing and delivery. *Commun. Mater.* **2**, 103 (2021).
- Fiorello, I., del Dottore, E., Tramacere, F. & Mazzolai, B. Taking inspiration from climbing plants: methodologies and benchmarks - a review. *Bioinspir. Biomim.* **15**, 031001 (2020).
- Stavriniidou, E. et al. In vivo polymerization and manufacturing of wires and supercapacitors in plants. *Proc. Natl Acad. Sci. USA* **114**, 2807–2812 (2017).
- Stavriniidou, E. et al. Electronic plants. *Sci. Adv.* **1**, 1501136 (2015).
- Neinhuis, C. & Barthlott, W. Characterization and distribution of water-repellent, self-cleaning plant surfaces. *Ann. Bot.* **79**, 667–677 (1997).
- Ensikat, H. J., Ditsche-Kuru, P., Neinhuis, C. & Barthlott, W. Superhydrophobicity in perfection: the outstanding properties of the lotus leaf. *Beilstein J. Nanotechnol.* **2**, 152–161 (2011).
- Koch, K., Bhushan, B. & Barthlott, W. Diversity of structure, morphology and wetting of plant surfaces. *Soft Matter* **4**, 1943–1963 (2008).
- Koch, K. & Barthlott, W. Superhydrophobic and superhydrophilic plant surfaces: an inspiration for biomimetic materials. *Philos. Trans. R. Soc. A Math. Phys. Eng. Sci.* **367**, 1487–1509 (2009).
- Heredia-Guerrero, J. A. et al. Infrared and Raman spectroscopic features of plant cuticles: a review. *Front. Plant Sci.* **5**, 305 (2014).
- Lin, S., Chen, X. & Wang, Z. L. Contact electrification at the liquid-solid interface. *Chem. Rev.* **122**, 5209–5232 (2022).
- Lee, J. W. & Hwang, W. Theoretical study of micro/nano roughness effect on water-solid triboelectrification with experimental approach. *Nano Energy* **52**, 315–322 (2018).
- Kim, J. H., Rothstein, J. P. & Shang, J. K. Dynamics of a flexible superhydrophobic surface during a drop impact. *Phys. Fluids* **30**, 072102 (2018).
- Vasileiou, T., Gerber, J., Prautzsch, J., Schutzius, T. M. & Poulikakos, D. Superhydrophobicity enhancement through substrate flexibility. *Proc. Natl Acad. Sci. USA* **113**, 13307–13312 (2016).
- Lee, J. B. & Lee, S. H. Dynamic wetting and spreading characteristics of a liquid droplet impinging on hydrophobic textured surfaces. *Langmuir* **27**, 6565–6573 (2011).
- Koch, K., Bhushan, B., Jung, Y. C. & Barthlott, W. Fabrication of artificial Lotus leaves and significance of hierarchical structure for superhydrophobicity and low adhesion. *Soft Matter* **5**, 1386–1393 (2009).
- Wagner, P., Fürstner, R., Barthlott, W. & Neinhuis, C. Quantitative assessment to the structural basis of water repellency in natural and technical surfaces. *J. Exp. Bot.* **54**, 1295–1303 (2003).
- Vasandani, P., Mao, Z.-H., Jia, W. & Sun, M. Relationship between triboelectric charge and contact force for two triboelectric layers. *J. Electrostat.* **90**, 157–162 (2017).
- Lacks, D. J. & Shinbrot, T. Long-standing and unresolved issues in triboelectric charging. *Nat. Rev. Chem.* **3**, 465–476 (2019).

53. Sosa, M. D. et al. Liquid-polymer triboelectricity: chemical mechanisms in the contact electrification process. *Soft Matter* **16**, 7040–7051 (2020).
54. Zhang, L. et al. Regulation and influence factors of triboelectricity at the solid-liquid interface. *Nano Energy* **78**, 105370 (2020).
55. Jeon, S. B., Seol, M. L., Kim, D., Park, S. J. & Choi, Y. K. Self-powered ion concentration sensor with triboelectricity from liquid–solid contact electrification. *Adv. Electron. Mater.* **2**, 1600006 (2016).
56. Hogrebe, A. M. R. & Mengel, K. in *Mechanisms and Effects of Pollutant-Transfer into Forests* 259–265 (Springer Netherlands, 1989).
57. Volkov, A. G. & Ranatunga, D. R. A. Plants as environmental biosensors. *Plant Signal. Behav.* **1**, 105–115 (2006).
58. Gunn, R. & Devin, C. Raindrop charge and electric field in active thunderstorms. *J. Meteorol.* **10**, 279–284 (1953).
59. Twomey, S. The electrification of individual cloud droplets. *Tellus* **8**, 445–452 (1956).
60. Gunn, R. Droplet-electrification processes and coagulation in stable and unstable clouds. *J. Atmos. Sci.* **12**, 511–518 (1955).
61. Wang, F. et al. Study of contact electrification at liquid-gas interface. *ACS Nano* **15**, 18206–18213 (2021).
62. Ensikat, H. J., Ditsche-Kuru, P. & Barthlott, W. in *Microscopy: Science, Technology, Applications and Education* (eds Mendez-Vliess, A. & Diaz, J.) 248–255 (Formatex Research Center, 2011).
63. Bouwkamp, C. J. & de Bruijn, N. G. The electrostatic field of a point charge inside a cylinder, in connection with wave guide theory. *J. Appl. Phys.* **18**, 562–577 (1947).

### Acknowledgements

This work was funded by the project GrowBot, the European Union's Horizon 2020 Research and Innovation Programme under grant agreement no. 824074.

### Author contributions

S.A. and F.M. designed and planned the experiments. S.A. carried out the experiments with the support of C.F.; S.A., F.M., and B.M. contributed to the interpretation of the results. F.M. and B.M. jointly supervised S.A.; S.A. and F.M. took the lead in writing the

manuscript with contributions from all authors. All authors provided critical feedback and helped outline the research, analysis, and manuscript.

### Competing interests

The authors declare no competing interests.

### Additional information

**Supplementary information** The online version contains supplementary material available at <https://doi.org/10.1038/s43246-022-00302-x>.

**Correspondence** and requests for materials should be addressed to Fabian Meder or Barbara Mazzolai.

**Peer review information** *Communications Materials* thanks the anonymous reviewers for their contribution to the peer review of this work. Primary handling editors: Bilge Baytekin and John Plummer. Peer reviewer reports are available.

**Reprints and permission information** is available at <http://www.nature.com/reprints>

**Publisher's note** Springer Nature remains neutral with regard to jurisdictional claims in published maps and institutional affiliations.



**Open Access** This article is licensed under a Creative Commons Attribution 4.0 International License, which permits use, sharing, adaptation, distribution and reproduction in any medium or format, as long as you give appropriate credit to the original author(s) and the source, provide a link to the Creative Commons license, and indicate if changes were made. The images or other third party material in this article are included in the article's Creative Commons license, unless indicated otherwise in a credit line to the material. If material is not included in the article's Creative Commons license and your intended use is not permitted by statutory regulation or exceeds the permitted use, you will need to obtain permission directly from the copyright holder. To view a copy of this license, visit <http://creativecommons.org/licenses/by/4.0/>.

© The Author(s) 2022